IAC-24-A6,IPB,11,x90608

POST-DOCKING SPACECRAFT SYSTEM IDENTIFICATION TO ENHANCE STACK ATTITUDE CONTROL

Mr. Giordano Benedetto Ugioli, Prof. Michèle Lavagna[a], Dr. Stefano Silvestrini[b], Mr. Lorenzo Capra[c]

[a] *Full Professor at Polytechnic of Milan*
[b] *Assistant Professor at Polytechnic of Milan*
[c] *PhD Student at Polytechnic of Milan*

Abstract

In light of numerous matured satellites in geosynchronous orbit that remain operationally capable but possess ageing ADCS, there has been a notable surge in interest regarding Orbit Servicing. The present work proposes a design and verification approach for the inertial and mechanical properties identification of an orbiting stack composed by two docked spacecrafts, with only one of the two being in charge of the composite attitude control. As a case study, the mission extension between MEV-1 and Intelsat-901 is considered, and CAD models of both satellites are developed to emulate the inertial data. The dynamic is simulated considering each satellite as a rigid body, while the docking is represented by a visco-elastic link. System identification is approached by considering a white box model and the family of data-fitting algorithms using Nonlinear Programming. The strategy here proposed sees two dynamical models of increasing complexity: a single body model, which considers the assembly as a whole spacecraft, and a double body model, which considers each spacecraft individually, exploited to simulate the attitude dynamics. The system identification procedure follows five sequential steps, each retrieving the inertial data fed in the next. The core of the proposed approach is based on the actuation of known torques and forces, and the sampling of rotational velocities data to regress on. The first three steps follow the simplification of the single body model to retrieve an accurate estimation of the inertia matrix and the center of mass of the whole assembly. The fourth and fifth steps retrieve the inertia properties of each body and the mechanical properties of the link between the two satellites respectively. The architecture is tested on different orbital conditions: Geosynchronous Earth Orbit and Medium Earth Orbit, to assess the error filtering capability of the fitting algorithm. A sensitivity analysis is carried out to explore the identification strategy robustness to uncertainties. Norm and orientation deviation in the control vector are considered, as well as angular velocity sensor measurements limited accuracy. The paper critically shows results on the use case adopted and on the test campaign occurred, to compare the control effectiveness before and after the identification procedures on different control modes: Inertial pointing, Repointing and Tracking. The control test certified an improvement in terms of time response after the system identification in each control mode, and a significant improvement in accuracy for inertial pointing mode.

Keywords: System Identification, Docking, Satellite, White Box, Numerical Methods.

Nomenclature

$Symbol$	Definition	Unit
a	Semi-major Axis	km
e	Eccentricity	-
i	Orbit Inclination	°
ω	Argument of the Perigee	°
Ω	Right Ascension of the Ascending Node	°
$\underline{r_i}$	Distance vector from Center of Mass	m
$A_{B/N}$	Rotation matrix from inertial to body frame	-
$A^T_{Btot/N}$	Rotation matrix from inertial to body frame of whole assembly	-
r_{CM-cm1}	Distance vector from CM_{tot} to CM_1	m
r_i'	Distance vector from CM_1 or CM_2	m
J_r	Sloshing inertia of first satellite	Kg m^2
θ_r	DoF of sloshing mass of the first satellite	°
C_r	Viscous parameter of the sloshing mass of the first satellite	Nms/rad
θ_1	Dof of first satellite	rad
J_l	Sloshing inertia of second satellite	kg m^2
θ_l	DoF of sloshing mass of the second satellite	rad
C_l	Viscous parameter of the sloshing mass of the second satellite	Nms/rad

M_{s1}	Disturbing torque from sloshing for first satellite	N m
M_{s2}	Disturbing torque from sloshing for second satellite	N m
J_{tot}	Total inertia for satellite assembly	kg m^2
θ_{tot}	Dof of the satellite assembly	rad
M_{tot}	Total torque acting on the satellite assembly	N m
J_{1cm}	Inertia matrix of the first satellite on the CM	kg m^2
J_{2cm}	Inertia matrix of the second satellite on the CM	kg m^2
K	Elastic parameter of the mechanical link	Nm/rad
C	Viscous parameter of the mechanical link	Nms/rad
M_{c1}	Control torque on first satellite	Nm
M_{ext1}	Disturbing torque on first satellite	Nm
M_{ext2}	Disturbing torque on second satellite	Nm
Δt	Time interval	S
M_x	Torque on x-axis	Nm
M_y	Torque on y-axis	Nm
M_z	Torque on z-axis	Nm
r_z	Z component of the lever arm	m
r_y	Y component of the lever arm	m
F_x	Force on x-axis	N
CM_2	Center of mass of the second satellite	m
CM_{tot}	Center of mass of satellite assembly	m
m_{tot}	Mass of satellite assembly	kg
CM_1	Center of mass of the first satellite	m
m_1	Mass of the first satellite	kg
m_2	Mass od the second satellite	kg
w_n	Natural frequency	rad/s
T_c	Control torque from control law	Nm
K_p	Proportional gain	-
w_e	Error angular velocity	rad/s
w_1	Angular velocity of the first satellite	rad/s
J	Generic inertia matrix	kg m^2
K_i	Integral gain	-
q_e	Quaternion error	-
$\Delta\theta_{max}$	Angular deformation between spacecraft	rad
e_1 e_2 e_3	Eigen axis	-
w_{lvlh}	Angular velocity of the LVLH frame	rad/s

1. Introduction

In the recent years, an increase in interest for the on-Orbit Servicing (oOS) activities has been recorded. Many satellites in Geosynchronous Earth Orbit are able to operate well beyond their design lives of 15 years and are decommissioned due to fuel depletion or ageing/malfunction of the Attitude Determination & Control (ADCS) rather than other subsystems. Replacing these "failing" satellites has a great cost in terms of design and launch, while the development of new technologies, such as electric propulsion, allow for the development of economically sound and safe oOS missions, capable of extending the operational life of several different spacecrafts.

Specifically, extending the mission operational lifetime means to dock with the target satellite, and then control the newly formed assembly. To generate an effective control after docking, the knowledge of the whole structure inertial parameters is required, which may either be provided by the ground or retrieved autonomously by the servicing spacecraft.

1.1 State of the Art

The estimation problem of the inertia matrix of a rigid body has been considered from several papers from the aerospace community, with least-squares method and different kinds of Kalman filters being the most used ones.

On the contrary, the present work follows the trail of data fitting algorithms [1], being based on white box model for system identification approach. In this work, the estimation is performed by combining analytical and numerical methods, Non Linear Programming(NLP). This results in a procedure that requires only the measure of the angular velocity, requiring no specific additional sensor or device.

1.2 Introduction to the problem

The Objective of the work is to define a series of experiments and algorithms to identify the properties of a system of two already docked satellites, in terms of inertial data and mechanical properties of the link connecting them.

The complete knowledge of the 1st Satellite is considered as available from the start in terms of: Inertia Matrix, position of the Center of Mass(CM), its own Mass, Position of the Thrusters, force and direction of thrusters.

Due to the broad applications available, the main driver to define the procedure has been identified in using only sensor and actuators commonly present inside the ADCS suites for spacecrafts, Inertial Measurements Unit(IMU), Gyroscopes, Momentum Exchange Device(MED) and Attitude thrusters. Moreover the 2nd satellite is considered as non-cooperative target, with no data transfer between the two.

1.3 Description of the Satellite Assembly

The Satellite Assembly is defined as composed from the 1st satellite, the active and controlling one, and by the 2nd satellite, which is the non-collaborative and passive satellite, connected by a mechanical Link.

The oOS Mission between Mission Extension Veichle 1(MEV-1) and Intelsat-901 has been chosen as case study to simulate and test the procedure.

2. Environment of Simulation and frames of Reference

2.1 Orbit Model

The orbit has been propagated using the restricted 2 body problem, not accounting for orbit disturbances since they do not impact the outcome of the procedure.

The orbital parameters of MEV-1 and Intelsat-901 oOS mission were chosen and are reported in Tab.1.

Table 1. Orbital Keplerian Parameters

a [km]	e [-]	i [deg°]	ω [deg°]	Ω[deg°]
42165	0.0002	1.64	345	132

2.2 Frames of Reference

Two main frames for the satellite assembly have been defined.

2.2.1 Body Frame

The Body Frame is centred in the geometrical center of the controlling spacecraft, with its main directions being parallel to the pitch, roll and yaw axis of the spacecraft. This is done for two reasons: the only available attitude is the one of the controlling spacecraft, and the position of the CM might change during the mission.

This frame is also used to evaluate the propagation of the kinematics using the quaternions.

2.2.2 Local Vertical Local Horizon

Defined by the orbit of the spacecraft, Local Vertical Local Horizontal (LVLH) frame is placed at the CM of the satellite. The x direction is directed from the CM of the Earth to the CM of the Spacecraft, while the z axis is normal to the orbital plane and y axis is the vector product between the two.

2.3 Disturbance

Disturbing Torques from environmental factor such as Solar Radiation Pressure(SRP), Gravity Gradient(GG), Magnetosphere and propellant sloshing are presented alongside the numerical integration since it affects the results and the repeatability of the results. The typical conditions of Geosynchronous Earth Orbit (GEO), similar to the one of the original oOS mission, together with the ones of Medium Earth Orbit(MEO) have been considered for the simulations to evaluate different levels of environmental disturbances.

2.3.1 Solar Radiating Pressure

SRP is generated by the interaction between the radiation emitted from the Sun and the surfaces of the spacecraft. The force has been modelled using the equation from[2] for the SRP model.

The disturbing torque is the cross product between the lever arm and the force, but since both spacecraft are free to rotate, the lever arm is defined as:

$$\underline{r_i} = A_{B/N} * A_{Btot/N}^{T} r_{CM-cm1} + r_i' \qquad (1)$$

The Sun Position has been evaluated in relation with the date of the docking, the 25th of February. The eclipsing condition has been modelled following [2], the shadow being regarded as having a conic shape, thus the condition for a total eclipse is the same as a transit from the apex of the shadow cone.

2.3.2 Gravity Gradient

The GG is generated by the interaction between Earth's gravity field and a non-symmetrical object of finite dimensions. In this case the Earth is considered as a perfect sphere, and the spacecraft assembly to be considered as a whole to avoid under/over estimation. The disturbing torque has been modelled following the equation from [2], and that can be decomposed for each body.

2.3.3 Magnetic Torque

The Magnetic Torque is result of the interaction between the residual magnetic field and Earth's Magnetosphere. In this case only the magnetic moment of the spacecraft are considered, since the other effects are considered negligible. The Magnetosphere on the other hand has been modelled as following the IGRF 2020 model [3] and using the magnetic dipole approximation, since the spacecrafts fly above 7000 km. The magnetic torque is evaluated as the cross product between the magnetic dipole of the spacecraft and the magnetic field in the body frame of each satellite.

2.3.4 Propellant Sloshing

Propellant sloshing is generated by the surface oscillations of a fluid in a partially filled tank. The resulting effects from the sloshing can be treated as the ones from ring dampener systems, hence a ring dampener on the Z axis of each satellite has been added with their respective CMs positioned on the geometrical center of each satellite.

The implementation of the disturbance requires to expand the Equation of Motion(EoM) of each satellite to add two Degree of Freedom(DoF):

$$\begin{cases} J_r\ddot{\theta}_r = C_r\left(\dot{\theta}_r - \dot{\theta}_1\right) \\ J_l\ddot{\theta}_l = C_l\left(\dot{\theta}_l - \dot{\theta}_2\right) \end{cases} \quad (2)$$

And the resulting disturbing torques:

$$\begin{cases} M_{s1} = C_r\left(\dot{\theta}_1 - \dot{\theta}_r\right) \\ M_{s2} = C_l\left(\dot{\theta}_2 - \dot{\theta}_l\right) \end{cases} \quad (3)$$

2.3.5 Numerical Simulation Options

Regarding the mathematical programming environment, Matlab and Simulink have been used to generate input data, elaborate numerical methods of NLP and post process the data. The version used is Matlab 2021b release.

Regarding the integration method, ODE45 was chose since it is adequate for non-stiff problems and provides a medium accuracy in providing the results.

3. Approach & Model

3.1 Modelling choices

Considering the issue if research of this work, the Rigid body model has been considered to approximate the behaviour of the spacecraft. In fact, using a structural body model would require the extensive knowledge of the second spacecraft and to identify the structure a distribute suite of sensors would be required, which is not available, considering that the two satellites cannot communicate.

3.2 Attitude Dynamical Model

Two model of increasing complexity have been created: Single Body Model(SBM) and Double Body Model(DBM). It is important to remark that the simulations are carried out using the DBM, while the SBM is only a used to define the reasoning behind some phases of the System Identification Procedure.

3.2.1 Single Body Model

The SBM is the first approximation and simplification of the problem, with the satellite assembly reduced to a single rigid body. This approach is valid under the assumption that the mechanical link between the two satellites ca be considered as rigid so that the forces exerted on the assembly induce very small deformations and that the effects from dynamics of appendages are negligible. The SBM follows the EoM:

$$J_{tot}\ddot{\theta}_{tot} = J_{tot}\dot{\theta}_{tot} \times \dot{\theta}_{tot} + M_{tot} \quad (4)$$

3.2.2 Double Body Model

The DBM is a more refined approximation, with the two different satellites being treated as two different bodies. In this case the mechanical connection is modelled as a set of 3 rotational springs and dampeners aligned with the principal axis of the body frame.

This approach is valid under the assumption that the relative translation between the two satellites is negligible and that the dynamics of the appendages are non-relevant.

The DBM follows the EoM:

$$\begin{cases} J_{1cm}\ddot{\theta}_1 = J_{1cm}\dot{\theta}_1 \times \dot{\theta}_1 + K(\theta_2 - \theta_1) + C\left(\dot{\theta}_2 - \dot{\theta}_1\right) + M_{c1} + M_{ext1} \\ J_{2cm}\ddot{\theta}_2 = J_{2cm}\dot{\theta}_2 \times \dot{\theta}_2 + K(\theta_1 - \theta_2) + C\left(\dot{\theta}_1 - \dot{\theta}_2\right) + M_{ext2} \end{cases} \quad (5)$$

3.2.3 Body Data

Notably, the only the masses and the general size of each spacecraft are available from launch press kits [4] and [5], to evaluate the inertia matrices, two Computer Aided Design(CAD) models were developed to obtain relevant data, while for the position of the CM, reasonable positions have been considered. Regarding the Mechanical link, the values have been chosen keeping in mind that a generic link between two satellites should be designed to be as rigid as possible, with high stiffness as priority, which would allow to treat the assembly, simplifying the control laws required.

4. System Identification Procedure

4.1 System identification approach

Considering that the basic rule in estimation is “not to estimate what you already know” and that the dynamical model of the attitude of the spacecraft is known and reported in the previous sections, the white box model has been chosen as approach for the system identification. Considering the communities around the core of system identification [6], the procedure here presented belongs to the family of “Fitting ODE-coefficients”, which takes advantage of the available physical modelling and fits well the white box approach.

4.2 Introduction to the Solution Logic

The idea behind the procedure, is to firstly identify the mass properties of the whole assembly by using a simplified dynamical model (SBM), then the properties of the connection between satellites are retrieved by using a more complex dynamical model (DBM).

The procedure is divided in 5 phases, the first three phases follow the hypotheses of the SBM, and their results are used in the remaining fourth and fifth phase, which follow the DBM model.

4.3 Phase I – Coarse Inertia

The first phase aims at providing a coarse estimation of the inertia matrix for the whole assembly.

Considering the EoM from the SBM, if the angular velocities are small, the term $J_{tot} w_{tot} \times w_{tot}$ inside Eq.4 becomes negligible. In this case the relationship between W_tot and the external torques becomes linearly dependant. Thanks to this property, it is possible to accelerate and brake the system, by applying the same torque for the same time in opposite directions. Integrating the EoM and rewriting the Eq it is possible to define:

$$J_{tot}^{-1} = (M_{tot} \Delta t)^{-1} w_{tot} \quad (6)$$

With 3 acceleration tests, one for each axis, it is possible to determine all the elements of the inertia matrix using the final value of the angular velocity.

4.3.1 Simulation and Results

Selecting the perturbing torque and the acceleration time is crucial to improve the quality of the results.

Both the torque generated by the first satellite and its acceleration time shall be greater than the one from the environmental disturbances but low enough to avoid exciting the non-linearities inside the EoM. From these evaluations, the values of 1Nm and 10 s have been selected.

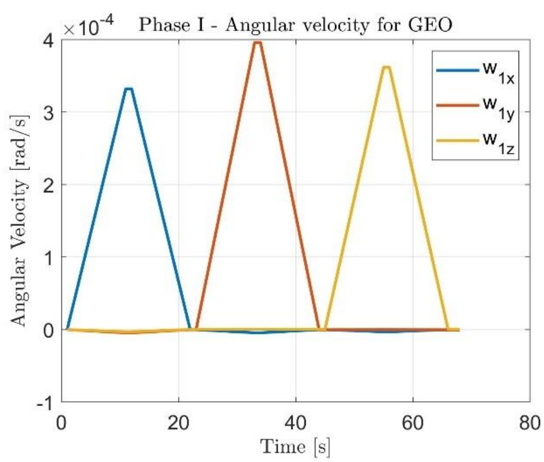

Fig.1. Angular velocity during 1st phase in GEO conditions

Analysing Fig.1 and Fig.2 it is possible to assess the linear increase and decrease in angular velocity with a constant torque and the increase in angular velocity offset during the 3 tests due to the MEO disturbance environment.

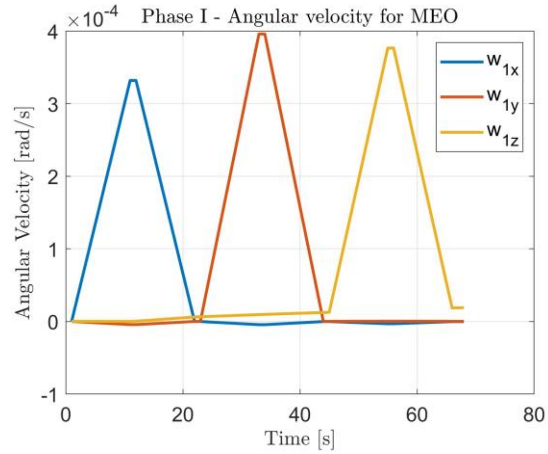

Fig.2. Angular velocity during 1st phase in MEO conditions

In Tab.2 the results of the 1st phase are presented, the increase in error is driven by the angular velocity offset present in Fig.2.

Tab.2.Estimation error of the inertia matrix in the 1st phase

$\boldsymbol{J_{tot}}$ Estimation	Norm of the diagonal error [kg m2]	Norm of the extra-diagonal error [kg m2]
GEO	37.04	21.04
MEO	1120	623.7

4.4 Phase II – Refined Inertia

The second phase refines the estimation of the inertia matrix for the whole assembly. It exploits the non-linearity of the equation of motion by applying a set of constant torques to the assembly. During the acceleration, the angular velocity profile gets sampled and is taken as a parameter inside the algorithm Inertia Refiner(IR). IR is an algorithm that optimizes a cost function through NLP constrained numerical method. The cost function takes as optimization parameter J_{TOT}, using the coarse estimation from phase 1 as starting guess, and defines the error as the difference between the sampled angular velocity and the propagated angular velocity during the acceleration. This phase allows to filter out disturbances while enforcing the symmetricity of the inertia matrix.

4.4.1 Simulation and Results

Parameters such as: Torque, Acceleration time, Sample time and Algorithm precision influence the quality of the results and have to be chosen carefully.

The torque generated by the first spacecraft shall be greater than the one from the environmental disturbances and excite the non-linearities inside the EoM but avoid exciting the visco-elastic components.

Acceleration time has to take into account that non-linearities arise over time, but a long acceleration time requires a greater number of samples, which might result in a stiffer problem.

Sample time must take into consideration the Shannon-Nyquist theorem and that the system starts from a linear response transitioning to a non-linear response, meaning that the frequency chosen is valid up to a certain angular velocity.

Algorithm precision is set by selecting the right constrained optimizer together with the propagation options. In this case a gradient constrained optimizer has been selected, using the built-in function of *FMINCON* inside Matlab, while a Runge-Kutta propagator, in the form of pre-built function *ODE45*, has been selected to propagate the angular velocity behaviour.

From these evaluations, the values of $M_c = [1\ 2\ 3]^T Nm$ for the Torque, 20s for the acceleration time and 5Hz as sample time have been considered.

In Fig.3 the error between the sampled and propagated angular velocity developed from the solution of the IR algorithm is shown, proving the ability of the algorithm to fit the behaviour of the spacecraft assembly. The error is greater on Z axis due to the greater torque being exerted, and due to the presence of the sloshing masses on the same axis.

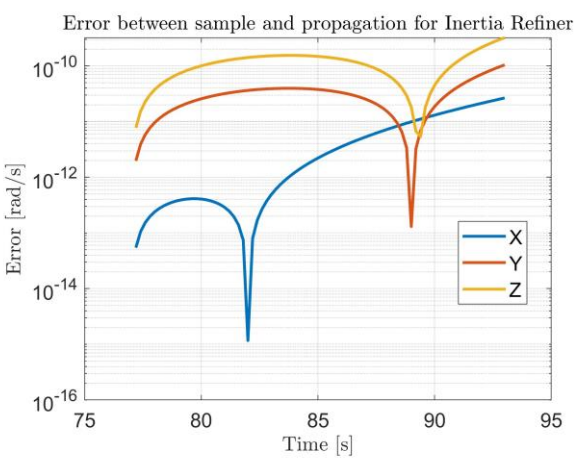

Fig.3. Logarithmic error between sample and propagated angular velocity

The results on the 2nd phase of the procedure are shown in Tab.3. It can be seen as the refining procedure is successful, since the estimation error is reduced, proving the capability of filtering out disturbances.

Tab.3. Estimation error of the inertia matrix in 2nd phase

J_{tot} Estimation	Norm of the diagonal error [kg m2]	Norm of the extra-diagonal error [kg m2]	Error Reduction [%]
GEO	1.36	2.11	96%
MEO	103.4	29.53	91%

4.5 Phase III – Center of Mass

The CM of the spacecraft defines the torque deriving from the force applied to the spacecraft. In this sense, the estimation of the CM can be carried out using the thrusters from the ADCS. Using the same reasoning of the first phase of the procedure, it is possible to perturb a spacecraft and maintain a linear relation between torque and angular velocity as in Eq.6. In this case the relation can be used to evaluate the torque applied to the system.

$$M_{tot} = (J_{tot}^{-1}\Delta t)^{-1} w_{tot} \qquad (7)$$

Due to the nature of the cross product between the lever arm and the force, it is possible to recover the lever arm if the force is applied aligned with one of the main axis of the system. In this way with one acceleration test it is possible to evaluate the lever arm components perpendicular to the force direction, as in the example of Eq:

$$\begin{cases} M_x = 0 \\ M_y = \frac{r_z}{F_x} \\ M_z = \frac{-r_y}{F_x} \end{cases} \qquad (8)$$

With two acceleration tests is possible to retrieve all 3 components of the lever arm between the CM and the position of the thruster. At this point a vectorial difference defines the position of the CM in the body reference frame.

Similarly to the SRP, the real torque during the simulation can be attained by using Eq.1 to allow for the relative rotation between the bodies.

4.5.1 Simulation and Results

Selecting the thruster torque and the acceleration time is fundamental in determining the quality of the results.

Both the torque generated by the first satellite and its acceleration time shall be greater than the one from the environmental disturbances but low enough to avoid exciting the non-linearities inside the EoM. In the case of thrusters, it is not possible to determine the real torque, but considering the scarcity of the fuel, low thrust actuators shall be considered. From these evaluations, the values of 0.1N and 10 s have been selected.

In Fig.4 the angular velocity profile during the 3rd phase is shown, where the linearity behaviour can be appreciated, validating the reasoning of the 3rd phase. In this case between one test and the other, a detumbling control has been applied, reducing the drift effects, as compared to the 1st phase.

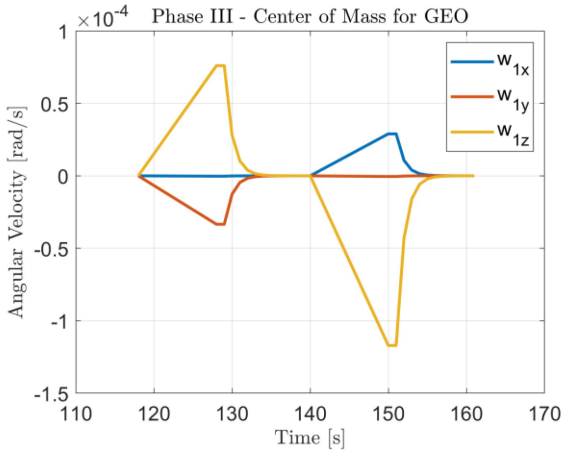

Fig.4 Angular velocities during the 3rd phase

The final results of the 3rd phase can be seen in Tab.4. The loss of CM position accuracy is not only connected to the increase in disturbances but can be mainly linked to the reduction of the estimation of the inertia matrix.

Tab.4. Estimation error of the CM

CM Estimation	Norm of the Error [m]	Relative error
GEO	0.01	2.7%
MEO	0.14	29.6%

4.6 Phase IV – Docked Spacecraft properties

The fourth phase of the procedure is only a mathematical one and aims at retrieving the individual properties of each satellite. No test is required for this phase.

Using the Huygens-Steiner theorem it is possible to evaluate the inertia matrix of the first satellite in the CM_{TOT}, and by difference with J_{TOT}, the inertia matrix of the second satellite in the CM_{TOT}. which are required to evaluate the DBM.

Second Satellite system identification: Additional data can be retrieved for the second satellite, which is grouped here since it is output from the procedure but does not affect the 5th phase.

Considering the 3rd phase, during the thruster firing, the acceleration can be recorded from the accelerometers present in the IMU. From the second principle of the dynamics, it is possible to evaluate the total mass of the Assembly from the force applied and the acceleration recorded. In this way the mass of the second satellite can be found as difference between the total mass and the mass of the first spacecraft. Once M2 is found, it is possible to evaluate the position of CM2 by using the definition of CM:

$$CM_2 = \frac{CM_{tot}m_{tot} - CM_1 m_1}{m_2} \qquad (9)$$

And by applying the Huygens-Steiner, recover J2.

This part of the procedure is just speculative, since translational dynamics is not evaluated inside the simulator. Furthermore, the simulation and the evaluation would use the same data and formula, generating perfect results every time, rendering useless the need for a simulation.

4.6.1 Simulation and Results

For this phase no simulation options are available.

In Tab.5 and Tab.6 the results of the 4th phase are shown. The error is directly related to the one of the previous phases, increasing with the disturbance level, and in a symmetrical pattern.

Tab.5. Estimation error in inertia matrix for the first satellite

J_{1cm} Estimation	Norm of the Diagonal Error [kg m2]	Norm of the Extra-diagonal Error [kg m2]
GEO	21.4	26.6
MEO	792	281.3

Tab.6. Estimation error in inertia matrix for the second satellite

J_{2cm} Estimation	Norm of the Diagonal Error [kg m2]	Norm of the Extra-diagonal Error [kg m2]
GEO	20.35	25.35
MEO	747	270

4.7 Phase V – Visco – Elastic Fitting

The fifth phase of the system identification procedure aims at identifying the viscous and elastic coefficients of the torsional spring and dampener system that connects the two spacecrafts. This is done by taking advantage of the high non-linearity terms inside the DoF of the DBM by applying a set of constant but different torques and performing an acceleration test.

Before the start of the acceleration, the spacecraft needs to reach zero angular velocity, by applying a detumbling control. In this way the angular velocity for both spacecrafts can be assumed to be zero, which is fundamental for the second spacecraft, since no measure is available.

The Spacecraft is then accelerated, and the angular velocity profile of the first spacecraft is sampled, to be used inside the algorithm.

The algorithm is called “Visco-Elastic Fitting” and uses a nonlinear least-squares solver and defines the parameters K and C as optimization variables. The cost function propagates the dynamics using using the EoM of the DBM and zero angular velocity for both bodies as initial condition. The error is then evaluated as the difference between the angular velocity sampled and the one propagated of the first satellite during the acceleration.

During the development of the work, two peculiarities have arisen which define the field of application of the method:

Rigid body threshold: the stiffness and damping coefficients must be compatible within 3 orders of magnitude of the inertia matrix, otherwise the solver will not be able to converge to a solution. Above certain level of stiffness, the system behaves as a whole rigid body, making the solver unable to converge, while under a certain level of stiffness the system behaves as two different uncoupled bodies.

Initial guess not required: it is not required to provide a reasonable initial guess for K and C for the optimizer to converge, but it is necessary that the initial guess respects the rigid body threshold. As a matter of fact, J_{TOT} diagonal elements might be taken in this case as initial guess, avoiding the need for an additional tests or specific sensors to generate the initial guess.

4.7.1 Simulation and Results

Similarly to the 2nd Phase, Torque, Acceleration time, Sample time and Algorithm options are crucial in defining the quality of the results.

The perturbing torque has to excite the dynamical and visco-elastic nonlinearities inside the EoM. In this case it is necessary to exert greater torque than before, keeping in mind as upper limit the torque available from available actuators and that a with high level of torque the propagation might lose precision, increasing the computational burden. A value of $M_c = [10\ 20\ 30]^T Nm$ Nm has been considered.

For the acceleration time, visco-elastic nonlinearities are more relevant at the beginning of the acceleration. Thus, a value of 10s has been chosen

Regarding the sample time, as in the 2nd phase it is important to respect the Shannon-Nyquist theorem. The maximum frequency of the system can be retrieved by looking at the natural frequency of the system defined as:

$$w_n = \sqrt{\frac{K}{J_{tot}}} \tag{10}$$

If the values of K are in a neighbourhood of 3 orders of magnitude, the ratio K/J_{TOT} should be around 10^2 Hz, hence the natural maximum frequency shall be smaller than 10 Hz. Considering the values in the simulation, a value of 0.1 s as sample time has been considered, to speed up the simulation.

Considering the algorithm precision, a non-linear least-squares curve fitting algorithm, in the form of the built in function of *LSQNONLIN* from Matlab, since it allows to evaluate the error at every step of the propagation. For the propagation, a Runge-Kutta algorithm in the form of the built-in function from Matlab *ODE45* has been considered for its flexibility between stiff and non-stiff problems. To speed up the process, the values of the diagonal of the J_{TOT} matrix have been considered.

Tab.7 Estimation error for the Elastic component

K (Elastic) Estimation	Norm of the Error [Nm/rad]	Relative error
GEO	6.7 10^3	0.6%
MEO	9.4 10^4	10.4%

Tab.8 Estimation error for the Viscous component

C (Viscous) Estimation	Norm of the Error [Nm s/rad]	Relative error
GEO	4.5 10^2	0.5%
MEO	1.33 10^4	14.4%

In Tab.7 and Tab.8, the results of the 5th Phase of the System Identification Procedure are shown, with a big leap between the GEO and MEO cases, due to error accumulation and increase in environmental disturbances.

In Fig.5 the logarithmic error between the sampled and propagated angular velocity profile is shown, proving the capability of the algorithm to fit the behaviour of the Spacecraft Assembly.

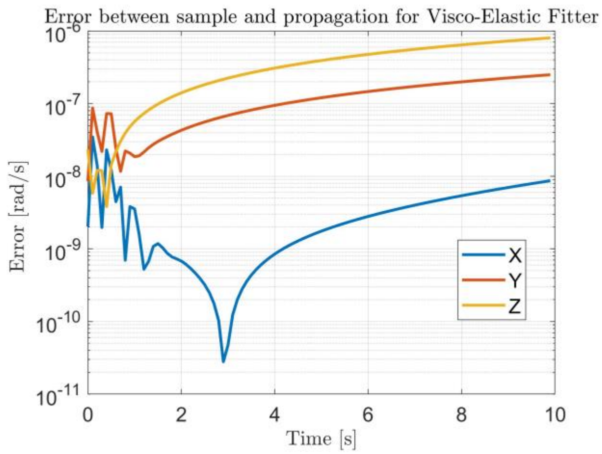

Fig.5. Logarithmic error between sampled and propagated angular velocity during the 5th phase

5. Sensibility and Control Performance analysis

5.1 Sensibility Analysis

To understand the robustness and limitations of the System Identification Procedure, a sensibility analysis has been carried out, using the reference GEO disturbance model.

5.1.1 Torque Delivery Mismatch

The Torque delivery mismatch considers a range of +-5% of the actual required torque. In Fig.6 the error behaviour for each relevant data from the system identification is shown.

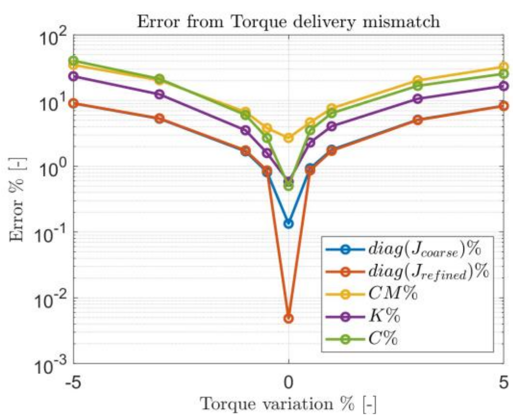

Fig.6. Estimation error due to Torque delivery mismatch

It is possible to notice that above 0.5% the error increases significantly for all of the estimations and the symmetrical fashion of it. Notably the IR algorithm is not able to improve the estimation of the inertia matrix, since the introduced error is greater than the environmental one.

5.1.2 Thrust Delivery Mismatch

Similarly to the Torque mismatch, a range of +-5% of the Thrust have been taken into account.

In Fig.7 the sensibility analysis on the thrust mismatch is presented.

Fig.7. Estimation error due to Force delivery mismatch

As expected, the precision in thrust delivery drives the precision of the estimation of the CM, which in return affects the individual inertia matrices. Thus, the error in estimating the Visco-Elastic components follows the same trend as the CM.

5.1.3 Torque Misalignment

If the exact alignment of the axis is not accurate, large errors in output torques may impact the attitude of the spacecraft [7]. To simulate the effects of a misaligned torque, the misalignment model for a set of three reaction wheels have been taken into consideration [8,9], since it allows to directly control the misalignment by using deviation angles. In this case a Montecarlo analysis has been performed, using 100 set of 3 deviation angles with a normal distribution of 1° with zero mean, since it is important to study the behaviour for small misalignment angles.

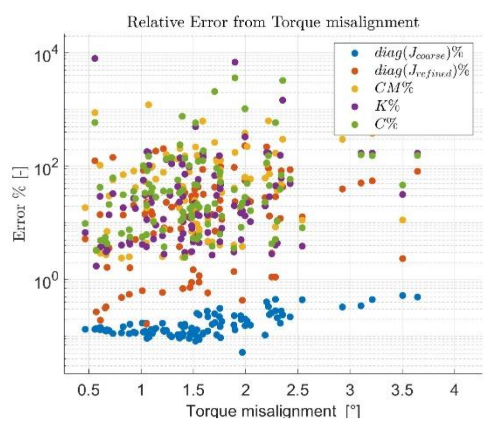

Fig.8 Monte Carlo Analysis of the estimation error due to Torque misalignment

In Fig.8 the results of the Montecarlo analysis for the torque misalignment is shown.

It is important to notice that the coarse estimation of the inertia matrix is does not suffer from the increase in angular deviation of the torque and provides a better estimation of the refined one. On the other hand the accuracy behaviour of the IR and Visco-Elastic Fitter algorithm is similar, since they both involve numerical optimization and have greater torque on z axis, meaning that the misalignment on this axis has a greater impact on both.

Considering together Fig.6 and Fig.8 it can be stated that is the knowledge accuracy of the torque is insufficient; the IR is not able to provide a better estimation than the coarse one.

5.1.4 Thrust Misalignment

To simulate the misalignment of the thruster force, rotation matrices have been developed to take into account the deviation angles as used in [10,11]. A Montecarlo analysis of 100 samples has been carried out, by considering a normal distribution with zero mean and 1° variance, to study the behaviour around the zero-deviation angle.

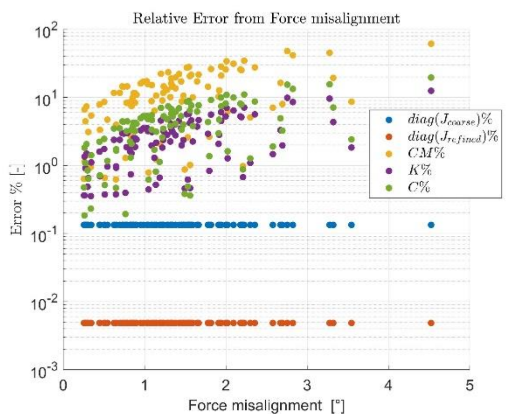

Fig.9. Monte Carlo analysis of the estimation error due to Torque misalignment

In Fig.9 the results of the Montecarlo analysis for the Thrust misalignment are shown. The estimation error for the CM increases linearly with angular deviation, while, as expected, the estimation of the Visco-Elastic components increases with similar fashion. On the other side, the error increase for K and C is not as steep as the one of the CM, suggesting that the Visco-Elastic Fitter algorithm is capable of filtering out not only disturbances, but also inaccurate data.

5.1.5 Angular Velocity Offset Error

Offset Error has been simulated as a fixed source of error to be added to the angular velocity measurement. Considering the angular velocities reached during the estimation process, a range between 10^-4 rad/s and 10^-8 rad/s has been used.

The results for the angular velocity offset sensibility analysis are shown in Fig.10.

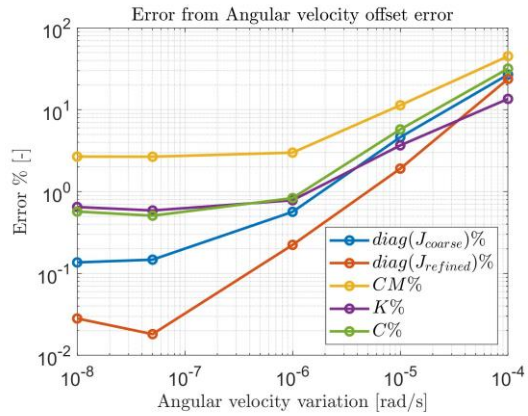

Fig.10. Estimation error behaviour due to angular velocity offset error

It can be seen that the relative error changes in a similar fashion for each estimation, and a threshold at 10^-6 rad/s is present, meaning that the offset error become similar to the actual angular velocity. Moreover the IR is always capable of improving the inertia matrix estimation, and the K and C estimation algorithm is capable of filtering the offset error and the one of the CM.

5.1.6 Angular Velocity Noise Error

In this case a random source of error has been added to the angular velocity measure, using a normal distribution with zero mean and a set of variances between 10^-4 rad/s and 10^-8 rad/s. In Fig.11 the results for the Angular velocity noise sensibility error are shown.

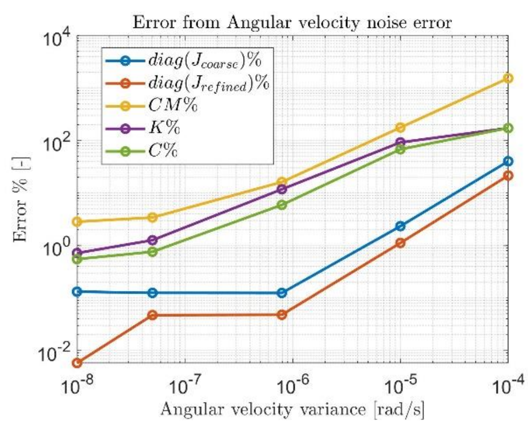

Fig.11. Estimation error behaviour due to angular velocity noise error

A threshold on 10^-6 rad/s can be seen. For smaller values of variance the coarse and refined estimations of the inertia matrix do not improve significantly, with a noise level similar to environmental disturbances. Moreover the K and C estimation is always able to improve the relative error compared to the CM estimation, rejecting estimation and noise error.

5.2 Control performance Comparison

To assess the utility of the new available data from the System Identification procedure, a set of control tests have been conducted. Two cases have been considered for the comparison, Before System Identification Procedure(BSIP) and After System Identification Procedure(ASIP).

5.2.1 Inertial Pointing

The inertial pointing mode requires to follow a certain angular velocity over time. The family of Proportional Integrative Derivative(PID) controllers has been used, specifically a proportional control law is used for this mode:

$$T_c = -K_p w_e + w_1 \times J w_1 \qquad (11)$$

Parameters KP and J have been set equal to J1 in the BSIP case and to JTOT in the ASIP one.

5.2.1 Test and Results

A total of 2 test have been carried out, one with a target velocity only on x axis and one with a target velocity on each axis. Each test is divided into 2 phases, one with a steady angular velocity target and one with a parabolic change in target angular velocity. In Fig.12 is shown the error over time for the x-axis case and in Fig.13 the one for the xyz-axis case.

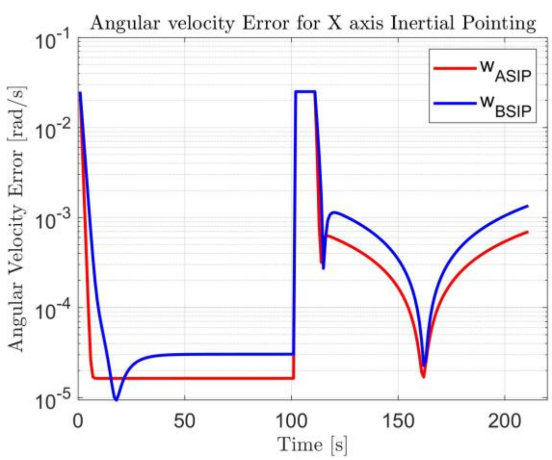

Fig.12 Angular velocity error over time for the inertial pointing mode on x-axis

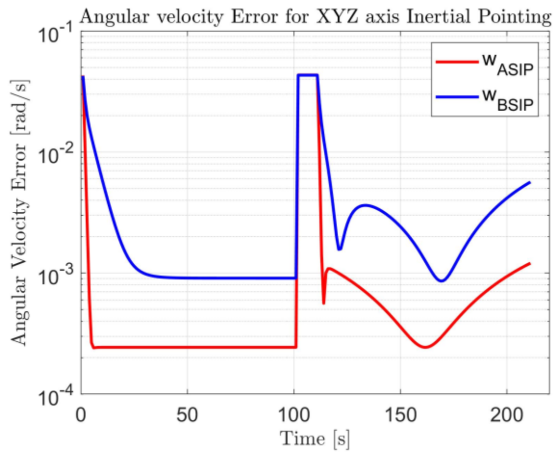

Fig.13 Angular velocity error over time for the inertial pointing mode on xyz-axis

For this control mode, ASIP improves the time responsiveness and the accuracy of the system, mainly due to the better compensation of the gyroscopic term.

5.2.2 Repointing

The repointing mode requires to perform a slew manoeuvre between two attitudes, to point a certain target (the Sun in this case). In this case a quaternion feedback control has been considered, and the gains treated as Proportional Integrative(PI) control law, as in [12]:

$$T_c = -K_i q_e - K_p w_1 + w_1 \times J w_1 \qquad (12)$$

For the execution of the tests, the parameters KI KP and J have been set equal to J1 for the BSIP case and to JTOT for the ASIP one.

5.2.2.1 Slew limit

To showcase the new possibilities and the usefulness of the retrieved data, a control constrain has been elaborated.

A classical slew manoeuvre is divided into 3 phases: acceleration, coasting and deceleration. In the coasting phase, the slew rate (i.e. the angular velocity) is constant and the acceleration is zero, and Eq.5 can be rewritten as:

$$\begin{cases} 0 = J_{1cm}\dot{\theta}_1 \times \dot{\theta}_1 + K(\theta_2 - \theta_1) + M_{ext} \\ 0 = J_{2cm}\dot{\theta}_2 \times \dot{\theta}_2 + K(\theta_1 - \theta_2) \end{cases} \qquad (13)$$

Implying the relation:

$$K(\theta_2 - \theta_1) = J_{2cm}\dot{\theta}_2 \times \dot{\theta}_2 \qquad (14)$$

Meaning that the angular difference between the two satellites during a slew motion is directly related to the slew rate, and limiting the angular difference means to impose a maximum slew rate constrain for the ASIP case. Due to the nature of the cross product, it is not possible to establish univocally a maximum angular velocity vector and using an if condition to evaluate the angular difference over time would be inefficient.

Considering the properties of the eigen axis:

$$\Delta\theta_{max} = \begin{bmatrix} e_1 \\ e_2 \\ e_3 \end{bmatrix} ||\Delta\theta_{max}|| \qquad (15)$$

$$w = \begin{bmatrix} e_1 \\ e_2 \\ e_3 \end{bmatrix} ||w|| \qquad (16)$$

And that Euler axis can be put into relation with the quaternion error vector at the beginning of the slew manoeuvre:

$$e_1 = \frac{|q_{1e}(0)|}{||q_e(0)||}\, e_2 = \frac{|q_{2e}(0)|}{||q_e(0)||}\, e_3 = \frac{|q_{3e}(0)|}{||q_e(0)||} \quad (17)$$

It is possible to rewrite Eq.14 and relate the maximum slew rate with the maximum angular difference:

$$\left|\left|\dot{\theta}_{max}\right|\right|^2 = \left(J_{2cm} \begin{bmatrix} e_1 \\ e_2 \\ e_3 \end{bmatrix} \times \begin{bmatrix} e_1 \\ e_2 \\ e_3 \end{bmatrix}\right)^{-1} K \begin{bmatrix} e_1 \\ e_2 \\ e_3 \end{bmatrix} ||\Delta\theta_{max}|| (18)$$

Once the maximum slew rate is defined, the control gains are defined as:

$$\begin{cases} K_p = J_{tot} \\ K_i = J_{tot} \frac{|q_{ie}(0)|}{||q_e(0)||} \left|\left|\dot{\theta}_{max}\right|\right| \end{cases} \qquad (19)$$

Providing a limited computational burden, since Eq.18 is evaluated one time only.

Once the manoeuvre is over, the control gains should be set again to JTOT to improve pointing accuracy.

5.2.2.2 Test and Results

The results for the repointing test in terms of pointing error is shown in Fig.14, while the angular velocity error in shown in Fig.13.

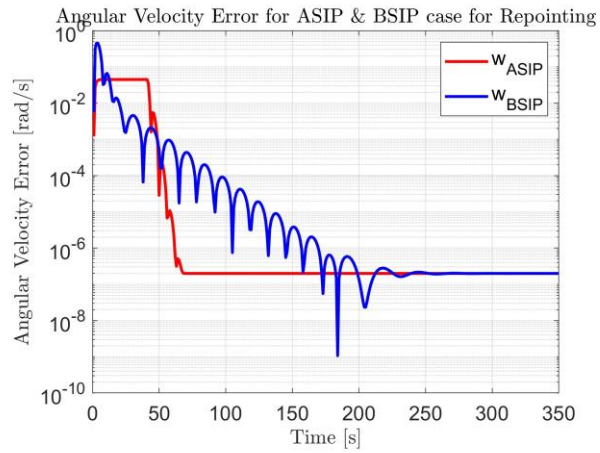

Fig.13 Angular velocity error during Repointing Mode

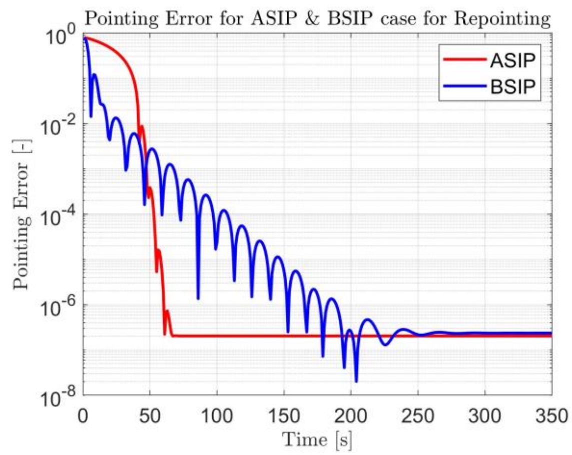

Fig.14. Pointing error during Repointing Mode

In this case the system identification procedure is able only to improve the response time and to reduce the oscillations during the slew manoeuvre, due to the cancellation of the gyroscopic term. In Fig.15, the angular difference between the two spacecrafts for the ASIP case is shown.

It can be seen that the maximum angular difference is respected, and that there are two spikes, which are expected, since the acceleration and braking are not accounted for inside the slew rate limit constrain model.

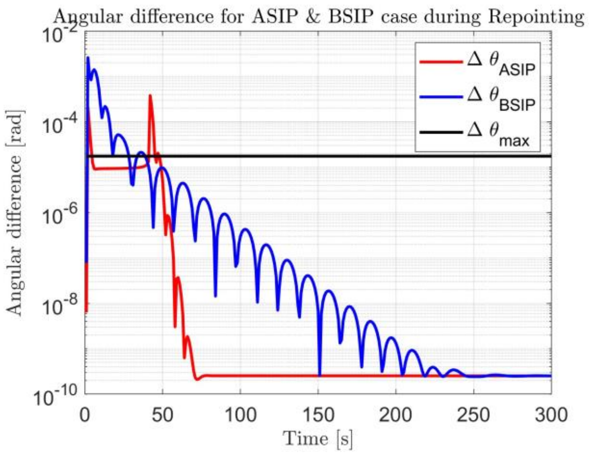

Fig.15. Angular difference between satellites during Repointing mode

5.2.3 Tracking

The tracking mode requires to follow a time-dependant attitude over time, following the LVLH frame as objective. In this case a quaternion feedback control law, as in Eq.12 has been chosen to carry out the test, with the angular velocity error defined as:

$$w_{err} = w_1 - A_{B/L} w_{lvlh} \qquad (20)$$

The control gains KI and KP, with the inertial term J have been considered equal to J1 for the BSIP case and to JTOT for the ASIP case.

5.2.3.1 Test and Results

The results for the tracking test in terms of pointing error is shown in Fig.16, while the angular velocity error in shown in Fig.17.

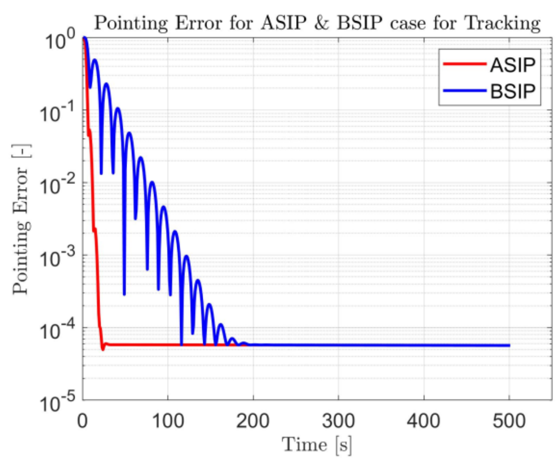

Fig.16. Pointing error during Tracking Mode

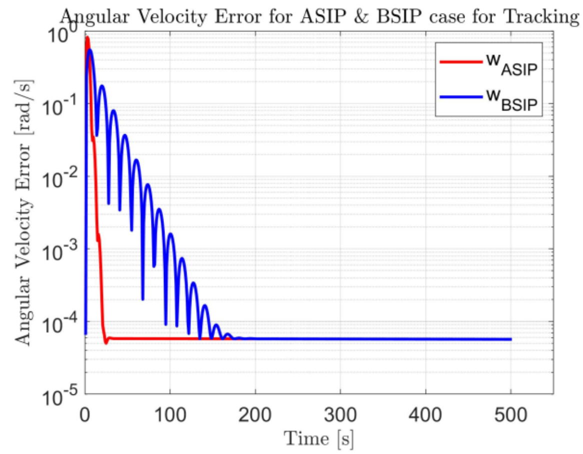

Fig.17. Angular velocity error during Tracking Mode

Similarly to the repointing test, only the oscillation and the response time are improved in the ASIP case.

6 Conclusion & Future Developments

The procedure found can be defined as capable of identifying the inertial and mechanical properties of two spacecrafts after their docking. It can also be assessed that the coarse estimation of the inertia matrix is more robust than the refined one in case of actuator flaws, and that on the other hand the refined estimation is capable to filter out not only environmental disturbances but also sensor flaws. The estimation of the visco-elastic parameters is strongly affected by the accuracy of the CM.

This identification procedure enhances the control accuracy by allowing the cancelling of the gyroscopic term inside the EoM, while allowing for the development of tailored control laws.

Regarding future developments, additional phases may be added with more complex dynamical models, such as the estimation of the inertial properties of the appendages and of the sloshing masses. Greater focus shall be added to specific phases that allow to reduce the build-up error and to exploit different kind of sensors and actuators.

References

[1] K. Schittkowski. Numerical data fitting in dynamical systems: a practical introduction with applications and software, volume 77. Springer Science & Business Media, 2002.

[2] J. R. Wertz. Spacecraft Attitude Determination and Control. KLUWER ACADEMIC PUBLISHERS, 2002

[3] I. A. of Geomagnetism and Aeronomy. Igrf online page. URL https://www.ngdc.noaa.gov/IAGA/vmod/igrf.html.

[4] Arianespace. Arianespace launchkit intelsat-901, 2001.

[5] Ilslaunch. E5wb/mev-1 mission overview, 2019.

[6] L. Ljung. Perspectives on system identification. Annual Reviews in Control, 34(1): 1–12, 2010.

[7] H. Yoon and P. Tsiotras. Adaptive spacecraft attitude tracking control with actuator uncertainties. The Journal of the Astronautical Sciences, 56(2):251–268, 2008

[8] W. Chen and Q. Hu. Sliding-mode-based attitude tracking control of spacecraft under reaction wheel uncertainties. IEEE/CAA Journal of Automatica Sinica, pages 1–13, 2022. doi: 10.1109/JAS.2022.105665.

[9] Q. Hu, B. Li, X. Huo, and Z. Shi. Spacecraft attitude tracking control under actuator magnitude deviation and misalignment. Aerospace Science and Technology, 28(1): 266–280, 2013

[10] B. Xiao, Q. Hu, D. Wang, and E. K. Poh. Attitude tracking control of rigid spacecraft with actuator misalignment and fault. IEEE Transactions on Control Systems Technology, 21(6):2360–2366, 2013

[11] H. Yoon, Y. Eun, and C. Park. Adaptive tracking control of spacecraft relative motion with mass and thruster uncertainties. Aerospace Science and Technology, 34: 75–83, 2014

[12] B. Wie. Space Veichle Dynamics and Control. American Institute of Aeronautics and Astronautics, Inc, 2008.